A statistical approach for spatial mapping and temporal forecasts of volcanic eruptions using monitoring data

Abani Patra[1,2], **Andrea Bevilacqua**[3], E. Bruce Pitman[2], Marcus Bursik[2], Barry Voight[4], Augusto Neri[3], Giovanni Macedonio[5], Franco Flandoli[6], Prospero De Martino[5], Flora Giudicepietro[5], Stefano Vitale[7,5].

(1) Tufts University, Medford, MA, (2) University at Buffalo , Buffalo, NY, (3) Istituto Nazionale di Geofisica e Vulcanologia, Pisa, Italia (4) Pennsylvania State University, State College, PA. (5) Istituto Nazionale di Geofisica e Vulcanologia, Napoli, Italia, (6) Scuola Normale Superiore, Pisa, Italia, (7) Università di Napoli Federico II, Napoli, Italia.

Paper Number V23I - 0321
Abstract ID: 602760

1. Introduction and overview

We present two models using monitoring data in the production of volcanic eruption forecasts.

- The **first model**, **in Section 2**, enhances the well-established **failure forecast method (FFM)** introducing a **stochastic differential equation** in its formulation. We provide **temporal** "*probabilistic predictions*", giving the user critical insight into a range of failure or eruption dates.

  In **Section 3**, using the new method, we describe an assessment of **failure time** on present-day unrest signals at **Campi Flegrei caldera** (Italy) using either **seismic count or ground deformation** data. The new formulation enables the estimation on decade-long time windows of data, including the effects of variable dynamics.

- The **second model**, **in Section 4,** establishes a Bayesian method to update vent opening **spatial** maps by **assimilating monitoring signals into a prior**, "*background*" vent opening map.

  The prior reproduces the two-dimensional distribution of past vent distribution with a **Gaussian Field**. The likelihood relies on a spatial variable characterizing the chance of material failure locally, based, for instance, on the horizontal ground deformation or on the local seismic count. We applied a new interpolation method to the GPS data, using **multiple points of central symmetry**.

  We describe examples based on the data collected in the **Campi Flegrei caldera** in the recent years by the monitoring network of INGV.

Let (x, t) ∈ $\mathbb{R}^3 \times \mathbb{R}_+$ be the spatial location and onset time of a **target phenomenon**.

A **volcanic precursor** is a real function F defined on a domain $A \times [t_0, t_1] \subseteq \mathbb{R}^3 \times \mathbb{R}_+$, such that F has a local maximum in (x, t).

Our purpose is to obtain **probability forecasts** of (x, t) given the values of F.

Depending on the additional hypotheses we can make on F, we describe two different cases (**Fig. 1**):

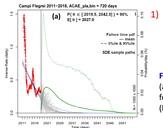

Figure 1. Examples of (a) enhanced failure forecast method and (b) posterior spatial map.

1) **Probabilistic enhancement of the Failure Forecast Method.**
Let the problem be temporal. Then F: $[t_0, t_1] \to \mathbb{R}$ is determined by a **physical equation** which links the rate X= dF/dt and the rate-change X. This provides estimates of the time t_f such that $F(t_f) = +\infty$.

2) **Update of a prior spatial map through the statistical assimilation of precursor data.**
Let the problem be spatial. Then the values of F: $A \to \mathbb{R}$ define a **likelihood map** which is combined with a prior probability distribution of (x,t) using the Bayes' Theorem.

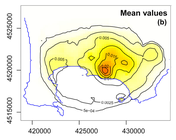

2. The Failure Forecast Method and its probabilistic formulation

The FFM is a well-established tool in the interpretation of monitoring data as possible **precursors**, providing quantitative predictions of a volcanic eruption onset (Voight, 1988).

The model represents the potential **cascade** of precursory signals leading to a significant rupture of materials, with t_f a proxy for the eruption onset t_e (**Fig. 2**).

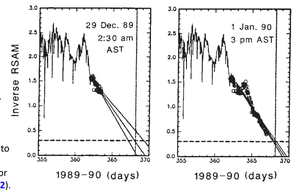

Figure 2. Examples of linear regression of the inverse rate of cascading seismic signals collected at Redoubt volcano (USA), before a major eruption in 1990 (from Voight & Cornelius, 1991)

The FFM has been retrospectively applied to several volcanic systems, including **explosive** eruptions. **Seismic** and **ground deformation** data are the type of signals most extensively studied with the method.

FFM is known to be affected by sources of **uncertainty**, like:
- the occurrence of multiple phases of acceleration in the signals
- the superposition of signals originating from different causes
- heterogeneity in the braking material, producing changes in the signals.

In addition, the statistical fitting of model parameters can be poorly constrained.

We perform a full probability assessment of FFM, with uncertainty quantification (**Fig. 3**).

$$dX/dt = AX^{\alpha}$$ where X is the time rate of signals

α - shape
A - slope
t_0 - initial time

$$X(t) = \left[(1-\alpha)A(t-t_0) + X(t_0)^{1-\alpha}\right]^{\frac{1}{1-\alpha}}$$ SOLUTION

γ - mean-reversion
σ - noise
β - initial perturbation

$$\eta := X^{1-\alpha} \xrightarrow[\text{linearization}]{\text{change of variables}} \frac{d\eta}{dt} = (1-\alpha)A$$

$$\eta(t) = (1-\alpha)A(t-t_0) + \eta(t_0)$$

t_f - failure time

$$t_f = \inf\{t : \eta(t) = 0\}$$

$$d\eta_t = \underbrace{\{\gamma\left[(1-\alpha)A(t-t_0) + \eta_{t_0} - \eta_t\right]}_{\text{mean-reversion terms}} + \underbrace{(1-\alpha)A\}\,dt}_{\text{classical FFM}} + \underbrace{\sigma dW_t}_{\text{noise term}}$$

$$X_t = \left\{X_{t_0}^{1-\alpha} + \int_{t_0}^{t}\left\{\gamma\left[(1-\alpha)A(s-t_0) + X_{t_0}^{1-\alpha} - X_s^{1-\alpha}\right] + (1-\alpha)A\right\}ds + \int_{t_0}^{t}\sigma dW_s\right\}^{\frac{1}{1-\alpha}}$$

Parameters are based on the residuals in the linearized problem.

NONLINEAR FORMULATION

$$t_f(\omega) = \inf\{t : X^{-1}(\omega, t) = 0\}$$

random variable

$$g_{t_f} : \mathbb{R} \to \mathbb{R}+, \quad \int_0^{\infty} g_{t_f}(x)dx = 1$$

t_f probability density function

In particular, we enhanced the classical FFM (see Bevilacqua et al., 2019) by:
- systematically **characterizing the uncertainty**, including both aleatoric sources (related to the future forecast) and epistemic sources (related to our current knowledge);
- **incorporating a stochastic noise** in the equations, and a mean-reversion property to constrain it (i.e. a Hull-white model).

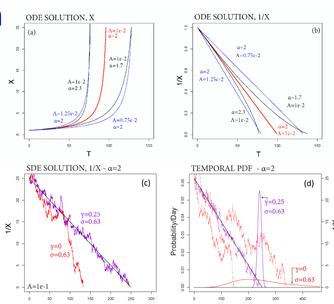

Figure 3. (a,b,) Classic FFM solutions, (a) X, and (b) 1/X. Note the effect of varying slope and convexity parameters.α, A learnt from data

(c, d) Stochastic FFM solutions, with α=2, A=0.1. The black line is the mean solution.
(c) colored lines are random paths, γ=0 or γ=0.25.
(d) also shows g_{t_f}. The solution 1/X is reported again.

4. Spatial updates of vent opening map through the assimilation of precursor data

LONG-TERM VENT OPENING MAP AT CAMPI FLEGREI

A vent opening map is a family of pdfs for the spatial location of a new eruptive vent (**Fig. 12**).
A hierarchical sampling is employed to choose the pdf and then the location.

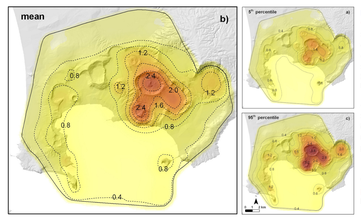

Figure 12. Vent opening map based on long-term volcanological data. The values are probabilities over km². (Bevilacqua et al., 2015, Bevilacqua, 2016)

A Gaussian random field can be adopted to represent the uncertainty affecting the pdf values.

We choose this field as a prior parameter for the Bayes' theorem.

GAUSSIAN FIELD REPRESENTATION OF THE VENT OPENING MAP

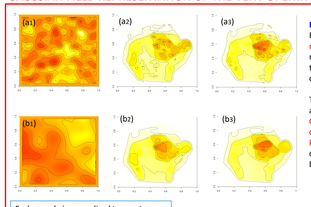

Figure 13. Example of random fields representing the vent opening map.

The plots assume Gaussian correlation kernels of different bandwidths.

Each sample is normalized to sum to one. Thanks to the law of large numbers, if correlation is not too strong, this is introducing a negligible error.

We assumed a radial limit of 4 km in the following, consistently with long-term correlation structure (Bevilacqua et al., 2015, Bevilacqua et al., 2016).

(a1-4) assume a radial limit of 2 km, (b1-3) of 5 km, i.e. beyond this radius the correlation is below 5% of its maximum value.

(a1, b1) display random samples of a Gaussian field with constant mean and unitary autocorrelation.
(a2-3, b2-3) show three random samples of a Gaussian field having the same 5th and 95th percentiles of the vent opening map in Bevilacqua et al. 2015, Bevilacqua et al., 2017.

Results are independent on arbitrary assumptions on the geometry, the physical properties of the source of deformation and of the elastic medium, but they are only based on a «local» central symmetry.

Centers of symmetry are locally determined for every pair of measurements, enabling the reconstruction of bimodal profiles, deviating from the bell-shape.

EXAMPLE OF THE NEW METHOD APPLIED TO SEISMIC DATA

Let X be the random variable expressing the new vent opening location according to the prior map g_0

Let F(x) be a likelihood function based on the distance from seismic epicenters. In this example we implement a Gaussian likelihood with 4 km radius (2σ). This is consistent with physical modeling of magmatic intrusion (Giudicepietro et al., 2017, Rivalta et al., 2019).

Then, let Y be a random variable with values in {0,1}, expressing the event of having an eruption after the observed precursors. That is, P(Y = 1 | X = x) is given by F(x).

The Bayes' theorem states:

$$g_{X\,|\,Y=h}(x) = \frac{P(Y=1\,|\,X=x)\,g_0(x)}{P(Y=1)} = \frac{F(x)\,g_0(x)}{h}$$

where the constant h is the Bayesian evidence that an eruption is going to happen, given prior and data.

If the observed signals are not real eruptive precursors, then

$$\forall\, x,\ P(Y=1\,|\,X=x) = P(Y=1) \equiv h,$$

$$g_{X\,|\,Y=h}(x) = g_0(x),$$

that is, the Bayes' theorem leaves the prior map unchanged.

So, we define a binary logic tree made of two cases:
A. The signals are real eruptive precursors
$g_{X\,|\,Y=1}(x) = \frac{F(x)\,g_0(x)}{h}$
B. The signals are not eruptive precursors
$g_{X\,|\,Y=h}(x) = g_0(x)$

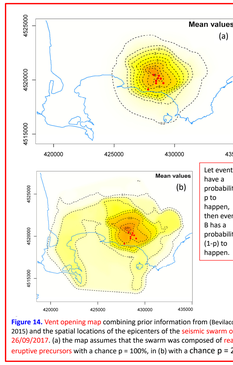

Figure 14. Vent opening map combining prior information from (Bevilacqua et al., 2015) and the spatial locations of the epicenters of the seismic swarm of 26/09/2017. (a) the map assumes that the swarm was composed of real eruptive precursors with a chance p = 100%, in (b) with a chance p = 20%.

MULTI-POLAR INTERPOLATION OF GPS MEASUREMENTS

Our spatial mapping of deformation data relies on a multi-polar interpolation, that is a linear interpolation among the pairs of applied vectors, made in polar coordinates with respect to the intersection of the straight lines defined by the horizontal displacement components.

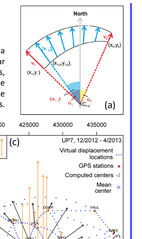

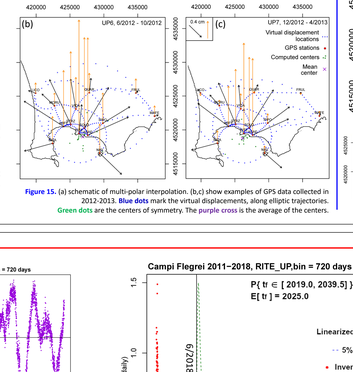

Figure 15. (a) schematic of multi-polar interpolation. (b,c) show examples of GPS data collected in 2012-2013. **Blue dots** mark the virtual displacements, along elliptic trajectories. **Green dots** are the centers of symmetry. The **purple cross** is the average of the centers.

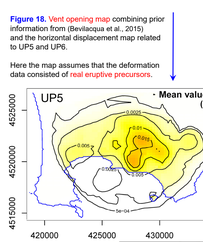

Figure 18. Vent opening map combining prior information from (Bevilacqua et al., 2015) and the horizontal displacement map related to UP5 and UP6.

Here the map assumes that the deformation data consisted of real eruptive precursors.

We focus our analysis on the minor uplifts (cm - scale) occurred in 2011-2013 (De Martino et al. 2014).

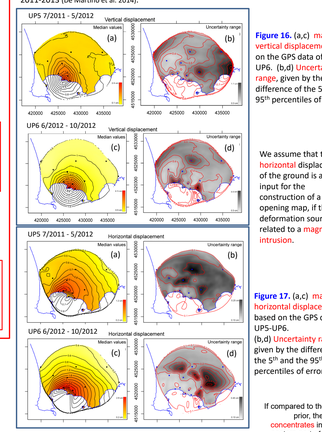

Figure 16. (a,c) maps of vertical displacement, based on the GPS data of UP5-UP6. (b,d) Uncertainty range, given by the difference of the 5th and the 95th percentiles of error.

We assume that the horizontal displacement of the ground is a key input for the construction of a vent opening map, if the deformation source is related to a magmatic intrusion.

Figure 17. (a,c) maps of horizontal displacement, based on the GPS data of UP5-UP6.
(b,d) Uncertainty range, given by the difference of the 5th and the 95th percentiles of error.

If compared to the long-term prior, the probability concentrates in the central eastern part of the caldera with a maximum corresponding to the zone of Solfatara crater.

There are multiple zones of increased vent opening probability on a wide subregion.

The probability was concentrated in the center-East.

EXAMPLE OF THE NEW METHOD APPLIED TO THE GROUND DEFORMATION

3. Temporal forecasts at the Campi Flegrei caldera using FFM

Campi Flegrei (Italy) is a **volcanic field** that has been active in the last 80'000 years. The depression of Campi Flegrei is generally interpreted as a **calderic structure**.

Two large scale collapses are related to the eruptions of:

-Campanian Ignimbrite (40'000 years BP); -Neapolitan Yellow Tuff (15'000 years BP)

The central part of the caldera has been uplifting in the last 10'500 years (a **caldera resurgence** of ~100 m).

Episodes of slow uplift and subsidence of the ground, called **bradyseism**, characterize the recent dynamics of the Campi Flegrei caldera (**Fig. 4, 5**).

In the last decades two major **bradiseismic crises** occurred in 1969/1972 and in 1982/1984, with a ground uplift of 1.70m and 1.85m, respectively.

Thousands of **earthquakes**, with a maximum magnitude of 4.2 caused the partial evacuation of the town of Pozzuoli in October 1983.

They were followed by about 20 years of overall subsidence, until 2005.

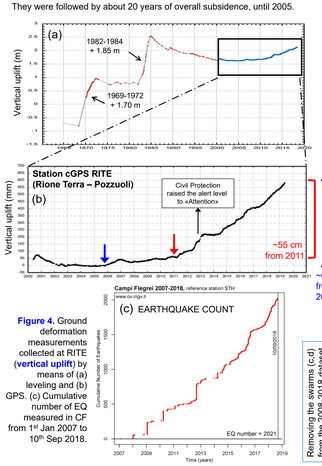

Figure 4. Ground deformation measurements collected at RITE (**vertical uplift**) by means of (a) leveling and (b) GPS. (c) Cumulative number of EQ measured in CF from 1st Jan 2007 to 10th Sep 2018.

Removing the swarms (c,d) from the 2008-2018 dataset significantly improves short-term forecasts.

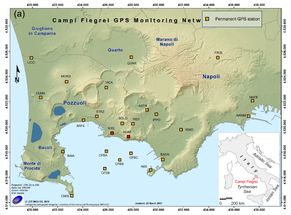

Figure 5. (a) Campi Flegrei caldera GPS monitoring network (21 stations + 4 buoys). RITE and ACAE stations marked in red.

(b) Plot of the elevation above sea level of the ruins of the Macellum of Pozzuoli (194 BC, called Serapeum Temple). Data reconstructed from the borings of marine organisms.

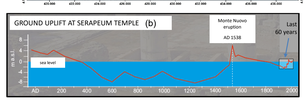

We preliminarily applied our enhanced FFM on Campi Flegrei caldera seismic and ground deformation dataset.

We remark that the time window is much longer than in the classical applications, and **spans over tens of years**.

FFM APPLIED ON THE EQ COUNT

t_f is the time when **accelerating signals** as observed in the last 10 years would diverge.

The interpretation of t_f as the onset of a volcanic eruption is **speculative** (Chiodini et al., 2017; Kilburn, 2018).

Figure 6. Probability forecasts of t_f using the seismic data of 2008-2018. In (a) the inverse rate is obtained on 120 days, in (b-d) on 360 days.

(b, d) are based on the data of 2011-2018, and (c, d) remove the swarms: $\forall i,\ t_{i+1} - t_i > 6$ hours.

Red points are inverse rate data. The **green line** is mean value of g_{t_f}, the probability/day scale bar is related to it. **Dashed lines** mark its 5th and 95th percentiles.

Thin blue dashed lines bound the 90% confidence interval of the classic FFM solution 1/X. A thin line is the mean path. **Grey dotted** lines display 50 stochastic solution paths.

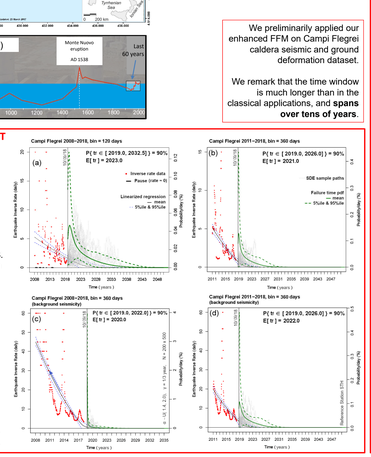

FFM APPLIED ON GROUND DEFORMATION DATA

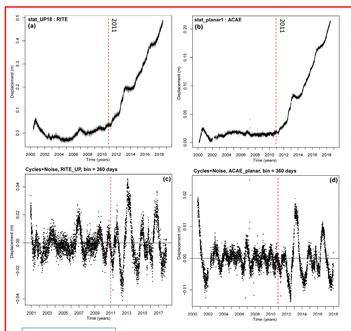

Figure 7. Ground deformation measurements of 2000-2018 collected at (a) RITE (vertical), and (b) ACAE (horizontal) GPS stations.

In (c-d) we show the **residual signal** after subtracting the average measurement over a 360 days moving window.

Seasonal cycles are evident, as well as noise effects.

Period and amplitude of the cycles apparently changed in 2011.

Rate change in 2011 is indicatively reported with a descriptive purpose.

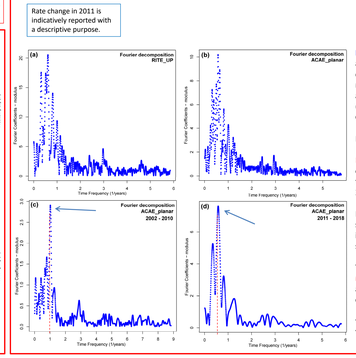

Figure 8. Fourier analysis of the residual deformation measurements collected at (a) RITE (vertical), and (b-d) ACAE (horizontal) GPS stations.

In (a-b) we show the $||\cdot||_2$ of Fourier coefficients, as obtained over the whole time domain 2000-2018.

In (c) we focus on the subdomain 2002-2010, in (d) on the 2011-2018 subdomain.

The period of the peak mode of the cycles appears to have changed:

~1 year in 2002-2010
~2 years in 2011-2018.

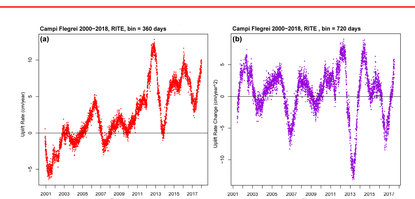

Figure 9. (a) Time rate of the deformation measurements collected at RITE (vertical) GPS stations, according to finite differences calculated over 360 days. (b) Rate change of the same time series, calculated by second order finite differences over 720 days.

Multiple phases of inverse rate decrease compatible with the FFM equations occurred in 2011-2013, and 2014-2016.

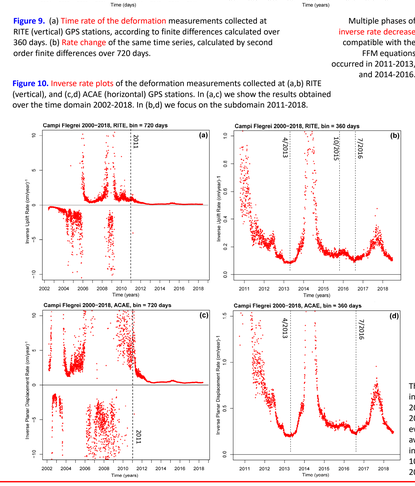

Figure 10. Inverse rate plots of the deformation measurements collected at (a,b) RITE (vertical), and (c,d) ACAE (horizontal) GPS stations. In (a,c) we show the results obtained over the time domain 2002-2018. In (b,d) we focus on the subdomain 2011-2018.

The minor uplift rate increases occurring in 2005-2006 and in 2011-2013 are evident, as well as the average rate, that increased up to above 10 cm/year in 2012-2013 and 2015-2016.

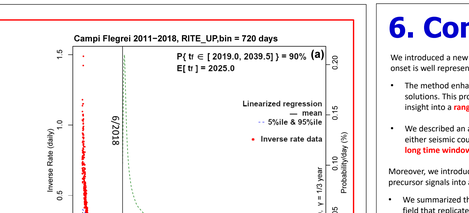

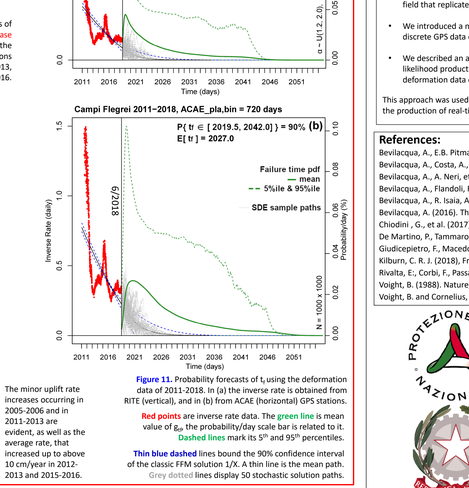

Figure 11. Probability forecasts of t_f using the deformation data of 2011-2018. In (a) the inverse rate is obtained from RITE (vertical), and in (b) from ACAE (horizontal) GPS stations.

Red points are inverse rate data. The **green line** is mean value of g_{t_f} the probability/day scale bar is related to it. **Dashed lines** mark its 5th and 95th percentiles.

Thin blue dashed lines bound the 90% confidence interval of the classic FFM solution 1/X. A thin line is the mean path. **Grey dotted** lines display 50 stochastic solution paths.

6. Conclusions

We introduced a new method for performing **short-term eruption timing probability** forecasts, when the eruption onset is well represented by a model of a significant rupture of materials.

- The method enhanced the well known FFM equation. We allowed **random excursions** from the classical solutions. This provided probabilistic forecasts instead of deterministic predictions, giving the user critical insight into a **range of failure or eruption dates**. More details in Bevilacqua et al., (2019).
- We described an assessment of failure time on **present-day unrest signals** at Campi Flegrei caldera (Italy) using either seismic count and ground deformation data. The new formulation enabled the estimation on **decade-long time windows** of data, locally including the effects of **variable dynamics**.

Moreover, we introduced a new framework for performing **short-term eruption spatial** forecasts by assimilating precursor signals into a prior ("background") vent opening map.

- We summarized the uncertainty affecting a **vent opening map pdf** by defining an appropriate Gaussian random field that replicates it.
- We introduced a new interpolation method based on **multiple points of central symmetry**, and we applied it on discrete GPS data collected at Campi Flegrei caldera.
- We described an application of the **Bayes' theorem** that combines the prior vent opening map and the data-based likelihood product-wise. We provide examples based on either seismic count and interpolated ground deformation data collected at Campi Flegrei caldera.

This approach was used during the **Civil Protection exercise EXEflegrei2019**, held in Oct 16-19. The method enabled the production of real-time vent opening maps using the monitoring signals provided (Bevilacqua et al., 2019b).

References:

Bevilacqua, A., E.B. Pitman, A. Patra, A. Neri, M. Bursik, B. Voight (2019), Front. Earth Sci. 7:135.
Bevilacqua, A., Costa, A., Macedonio, G., Neri, A., Sandri, L., Selva, J. (2019b), EXEflegrei2019, INGV_DPC.
Bevilacqua, A., A. Neri, et al. (2017), Front. Earth Sci., 5, 72, 1-16.
Bevilacqua, A., Flandoli, F., Neri, A., Isaia, R., Vitale, S., (2016). J. Geophys. Res. 121, 7821-7845.
Bevilacqua, A., R. Isaia, A. Neri, S. Vitale, et al., (2015), J. Geophys. Res., 120, 2309-2329.
Bevilacqua, A. (2016). Theses, 21. Edizioni della Normale, Birkhäuser/Springer.
Chiodini , G., et al. (2017). Scientific Reports, 7: 4472.
De Martino, P., Tammaro, U., Obrizzo, F., 2014. Annals of Geophysics, 57(2), S0213.
Giudicepietro, F., Macedonio, G., and Martini, M. (2017), Front. Earth Sci. 5:54.
Kilburn, C. R. J. (2018), Front. Earth Sci. 6:133.
Rivalta, E;, Corbi, F., Passarelli, L., Acocella, V., Davis, T., Di Vito M.A. (2019), Sci. Adv. ,EAAU9784.
Voight, B. (1988). Nature, 332:125-130.
Voight, B. and Cornelius, R. R. (1991). Nature, 350:695-698.

Acknowledgments:
This work is supported by the Department of Civil Protection through the agreement INGV-DPC contract 2019-2021, by the National Science Foundation award 1821313, and by the Italian Ministry of Research - project FISR2017.